Control of Oscillating Combustion and Measurements of Turbulent Flames

Mamoru TANAHASHI, Shinichiro MURAKAMI, Toshio MIYAUCHI
Department of Mechanical and Aerospace Engineering, Tokyo Institute of Technology, 2-12-1 Ookayama, Meguro-ku, Tokyo 152-8552, Japan

Gyung-Min CHOI
Japan Aerospace Exploration Agency, 7-44-1 Jindaiji-Higashi, Chofu, Tokyo 182-8522, Japan

To control combustion oscillations, the characteristics of oscillating premixed flame have been investigated and control of combustion oscillation and noise based on local flame structure has been conducted. The pressure fluctuations, which plays important roles in noise generation, could be controlled by injecting secondary fuel into the recirculation zone of oscillating flames. Injecting secondary fuel prevented lean blowout and low NOx emission was achieved even for the case of pure methane injection as a secondary fuel. Mixture injection instead of pure fuel is not effective for control of combustion oscillations and blowout prevention. By changing injection frequency of secondary fuel, the minimum value of r. m. s. of pressure fluctuations and noise has been achieved. The simultaneous CH-OH PLIF and stereoscopic PIV measurement have been developed to investigate the local flame structure of oscillating turbulent premixed flames. The developed simultaneous measurement of two radical concentrations and three velocity component on a two-dimensional plane was applied to relatively high Reynolds number turbulent premixed flames in a swirl-stabilized combustor. All measurements were conducted for methane-air premixed flames in the region of corrugated flamelets. Simultaneous CH and OH images suggest the presence of the isolated burned gas in the unburned mixture and the isolated unburned mixture in the burned side that have been predicted by direct numerical simulation of turbulent flames. Strong three-dimensional velocity fluctuations were measured by the stereoscopic PIV. Furthermore, comparisons of CH-OH PLIF and three-dimensional velocity field show that the burned gases not always have high-speed velocity in relatively high Reynolds number turbulent premixed flame. The Reynolds number dependence of flame front geometry was clearly captured by the simultaneous CH-OH PLIF and stereoscopic PIV measurement. This simultaneous CH-OH PLIF and stereoscopic PIV measurement system can be applicable to the investigation of the flame/turbulence interactions.

1. Introduction

It has been considered that most of combustion oscillations or combustion instabilities are caused by the feedback interaction between natural acoustic modes of combustor and oscillations of heat release rate (Rayleigh, 1945). Since such combustion oscillations or instabilities may cause noise emission and break down of the combustor, a number of studies have been conducted to make clear the mechanism and the control strategies of combustion oscillation (Samaniego, *et al.* 1993, Broda, *et al.* 1998, Di Benedetto, *et al.* 2002, Paschereit, *et al.* 1999, Lieuwen, *et al.* 2000, Gulati, *et al* 1992, Sivasegaram, *et al* 1995, Blonbou, *et al* 2000). From the viewpoint of pollution formation, NOx have a major impact on the environment and studies related to NOx reduction by passive or active control have also been conducted (Poppe, *et al*. 1998, Delabroy, *et al*. 1998, Murugappan, *et al*. 2000).

According to Rayleigh, we may easily control combustion oscillations by simply introducing an energy source out of phase with heat release rate. However, it has been demonstrated that successful control strategies use variations of combusting condition or combustors (Gulati, *et al.* 1992, Sivasegaram, *et al.* 1995, Blonbou, *et al.* 2000). Therefore, a detail understanding of the combustion oscillations and/or instability mechanism is necessary for an effective and robust active control of combustion. To obtain important factors for control of combustion oscillations, several experimental studies have been conducted for flame-acoustic interactions in unstable combustors using phase-locked measurements (Samaniego, *et al.* 1993, Broda, *et al.* 1998). Quantitative measurements of the flames response to acoustic perturbations have also been conducted (Poinsot, *et al*. 1986, Harper, *et al*. 2001). These measurements are heavily influenced by the combustion system. Since the heat release rate plays important roles in the sound generation mechanism in the turbulent combustion field (Tanahashi, *et al*. 2002a), it is very informative to identify the dominant sound source through the understanding of spatial and temporal fluctuations of the heat release rate in the combustor for the development of active control schemes.

Recently, the effect of secondary fuel injection location on the effectiveness of active combustion control was studied in a laboratory-scale dump combustor at atmospheric pressure (Lee, *et al*. 2000). And, simulation experiments have been conducted to evaluate the control law under wide-range operation of a generic combustor using secondary fuel injection (Hong, *et al*. 2002). Combustion control using secondary fuel injection has two advantages; one is that successful combustion control is possible using considerably small amount of energy and the second is that it reduces the actuator requirements. From these advantages, the secondary fuel injection method is desirable to suppress pressure fluctuations and to prevent lean blowout of the flame. On the other hand, optimum design has been required to minimize the amount of secondary fuel because it had been considered that secondary fuel injection might cause large amount of nitric oxide. In previous study (Tanahashi, *et al*. 2003b), we reported that a beating of pressure fluctuations was observed in the largely fluctuating combustion conditions and a certain relationship between local flame structure and pressure fluctuations was also investigated.

To control oscillating combustion effectively, it is necessary to investigate detailed information about local flame structure of turbulent flames. To investigate turbulent flame structures experimentally, planar laser induced fluorescence (PLIF) of OH radicals and CH radicals are commonly used (Dyer, *et al*. 1984, Hanson, 1986). Since OH radicals show high concentration in the burned gas, OH PLIF measurements are useful to separate the unburned mixture and the burned gas. Although the edges of OH radical distribution may correspond to the flame fronts for low Reynolds number turbulent flames, there is a possibility that the flame fronts do not exist at the edge of OH radicals in high Reynolds number cases in which flame front is significantly distorted and multiply folded. On the other hand, CH PLIF measurements have been used to investigate characteristics of the flame fronts in turbulence because CH radicals are produced at the flame front and have very narrow width enough to represent the reaction zones (Allen, *et al*. 1986, Mansour, *et al*. 1998, Carter, *et al*. 1998). Furthermore, it is well known that distribution of CH radicals agrees with that of the heat release rate (Paul, *et al*. 1998). However, it is hard to distinguish the unburned from burned gases by the CH-PLIF measurement. To overcome these defects, simultaneous OH and CH PLIF measurements have been developed and applied for turbulent non-premixed flames (Donbar, *et al*. 2000, Watson, *et al*. 2002). In addition to the PLIF measurements, particle image velocimetry (PIV) have been adopted to measure the turbulence characteristics near the flame (Kalt, *et al*. 1998, Rehm, *et al*. 1998, Han, *et al*. 2000, Sinibaldi, *et al*. 2003). Recently, simultaneous CH, OH and velocity measurement has been reported in non-premixed flame (Kothnur, *et al*. 2002). However, almost all studies used two-dimensional PIV to measure the velocity field. To obtain the detailed information about turbulent velocity field, three component velocity measurement such as the stereoscopic PIV (Arroyo, *et al*. 1991, Willert, 1997, Prasad, 2000) are desirable. In this study, to control local flame structure, we adopted secondary fuel injection in the swirl-stabilized premixed flames. Control using secondary fuel injection has been conducted to suppress flame oscillating and noise and to prevent lean blowout. Variations of emission index with secondary fuel injection were also measured. Also, simultaneous CH-OH PLIF and stereoscopic PIV measurement are developed to investigate the local flame structure of turbulent premixed flames. Simultaneous measurements of two radical concentrations and three component velocity are conducted at relatively high Reynolds number turbulent premixed flames in swirl-stabilized combustor and characteristics of flame geometry and its Reynolds number dependence are discussed.

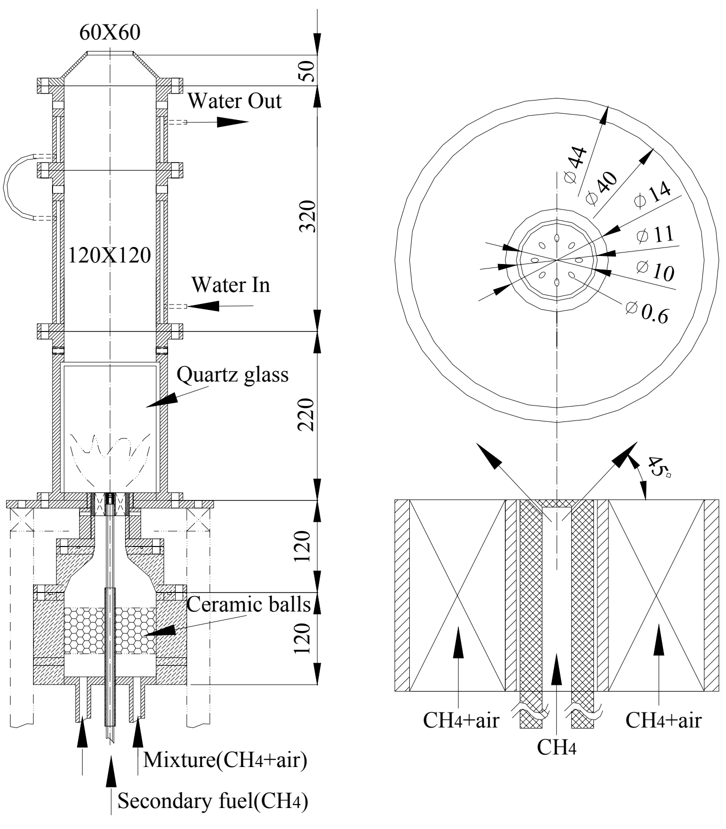

Fig. 1 Schematics of combustion system and details of swirler and secondary fuel nozzle

2. Control of oscillating combustion by secondary fuel injection

2.1 Experimental methods and conditions

Figure 1 shows schematics of swirl-stabilized premixed combustor and detail of secondary fuel injection nozzle. This combustion rig consists of contraction section, swirl injection section and combustion chamber. The inner diameter of 120mm is reduced to 40mm diameter in the contraction section. The inner cross-section of combustion chamber was 120mm × 120mm and the outlet of combustion chamber was contracted to 60mm × 60mm. The total length of combustion chamber was 590mm. On each side of combustion chamber, a silica glass plate of 120mm × 170mm and 5mm thickness was installed to allow optical access. The swirl injector has 14mm inner diameter and 40mm outer diameter, and swirl vanes are inclined 45 degrees from the streamwise direction. The secondary fuel nozzle was mounted at center of the swirl vanes, and there are 8 injection holes (I.D. =0.6mm) which is inclined 45 degrees from streamwise direction. The pressure transducer (TOYODA, PD104) was used to measure pressure fluctuations in the combustion chamber. A water-cooling connection tube was used to mount the pressure transducer at the position of 250mm downstream from the swirl vanes. Sound level was measured with microphone (ONO SOKKI, LA-1240) at the 1700mm height from ground and 300mm apart from the exit of combustion chamber when the height of combustor exit is about 1800mm from ground. The concentration of nitric oxides was measured by a chemiluminescence analyzer (SHIMADZU, NOA-7000). A water-cooled sampling probe with a 1.0mm suction hole was used to sample the burned gases at the 20mm upstream from the exit of combustion chamber. Because there are spatial fluctuations of NOx concentration as a consequence of oscillating combustion, the averaged value of three different points were used to calculate emission index. The flow rates of main mixture are varied from 200 to 300 *l*/min and equivalence ratios are varied from lean blowout limit to 1.3. Methane is used as fuel of main mixture and secondary fuel.

2.2 Combustion control by secondary fuel injection

Figure 2 shows pressure fluctuations with secondary fuel injection. Q_m, Q_{sf} and ϕ denote the mixture flow rate, secondary fuel flow rate and equivalence ratio, respectively. Regardless of mixture flow rates, the r. m. s. value of pressure fluctuations shows significantly large values between $\phi = 0.8$ and 1.1. For Q_m=200*l*/min, with increase of the secondary fuel injection, the r. m. s. of pressure fluctuations decreases monotonously. With increasing mixture flow rate, effect of secondary fuel on pressure fluctuations becomes weak. However,when the secondary fuel injection exceeds 1.5% of mixture flow rate, the r. m. s. of pressure fluctuations decreases drastically.

Figure 3 shows noise level with secondary fuel injection. Although the r. m. s. of pressure fluctuations increased with secondary fuel injection from 0.5% to 1.0% of secondary fuel injection, noise level decreased significantly when the secondary fuel exceeds 1.0% even though there are some increments of noise level at lean conditions. It can be seen that the noise level is decreased about 10dB for $\phi = 0.8$ - 1.0. Near $\phi = 0.8$ of Q_m= 300 *l*/min case, large noise level reduction of 20 dB is observed for 1.0%

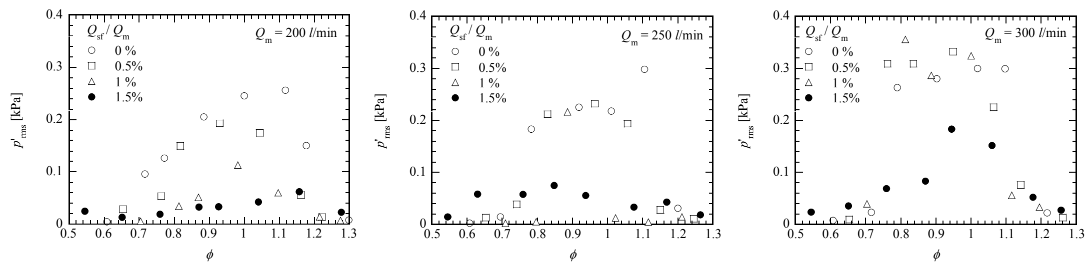

Fig. 2 Pressure fluctuations with secondary fuel injection

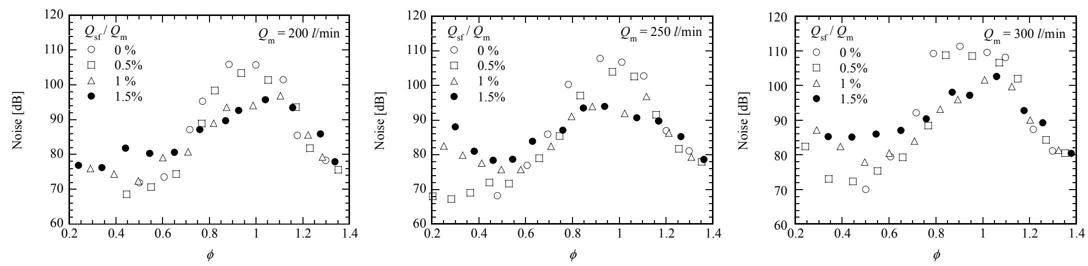

Fig. 3 Combustion noise with secondary fuel injection

secondary fuel injection, though the r. m. s. of pressure fluctuation is larger than that without secondary fuel condition. To investigate the mechanism of noise level reduction, power spectrum of pressure fluctuations with and without secondary fuel injection are compared in Fig. 4.

By injecting 1% secondary fuel, the neighboring peak in the power spectrum disappeared, where the energy at the dominant frequency with secondary fuel injection is larger than that without secondary fuel. This tendency can be observed even for ϕ = 0.9. The noise level reduction in Fig. 3 is ascribed to the elimination of beating of pressure fluctuations through the control of local flame structure by injecting secondary fuel. From the result of little effect in pressure fluctuations and noise level for 0.5% secondary fuel injection, it can be seen that there is a minimum flow rate of secondary fuel to control the local flame structure in the present swirl injection premixed combustor.

If the injected pure methane react as a diffusion flame, a large amount of nitric oxides will be produced. Figure 5 shows the variation of emission index with secondary fuel injection. For the case without secondary fuel injection, emission index also shows a large value in the region of large oscillation and noise for all flow rates conditions. This large amount of emission index is ascribed to the combustion oscillating with complicated flame structures. With the injection of secondary fuel, it is observed that the emission index decreases in the large pressure fluctuating region. However, effect of secondary fuel injection on lean and rich conditions is small. For 0.8 < ϕ < 1.1 and without secondary fuel injection, the flame stabilizes near swirl injector and locally intense reaction regions are observed. On the other hand, when secondary fuel is injected, the flame lifts slightly and relatively uniform and widespread flame is formed. Low emission index is ascribed to lifted, relatively uniform and widespread flame. In addition, the lean blowout limits are extended to quite lean condition by injecting secondary fuel. From the above result, it can be seen that secondary fuel injection is effective to suppress combustion oscillation, to prevent lean blowout and to reduce emission index.

Figure 6 shows influence of secondary premixed mixture injection on the r. m. s. of pressure fluctuations and noise with 1.0% secondary premixed mixture injection. Here, ζ_f is the ratio fuel flow rate to mixture one. To evaluate the effect, the results without secondary fuel injection are also plotted. R. m. s. of pressure fluctuations with secondary premixed mixture injection is less than that of pure methane secondary fuel injection under ϕ =1.0 conditions, though opposite tendency is observed over ϕ =1.0 conditions. For the noise level, secondary premixed mixture injection has little effect on noise reduction. But, the noise level with secondary premixed mixture injection seldom exceeds that without secondary fuel injection. The lean blowout limit moved to rich side with increasing air amount in the secondary premixed mixture. These results demonstrate that secondary premixed mixture injection is not effective for control of combustion oscillations and lean blowout prevention.

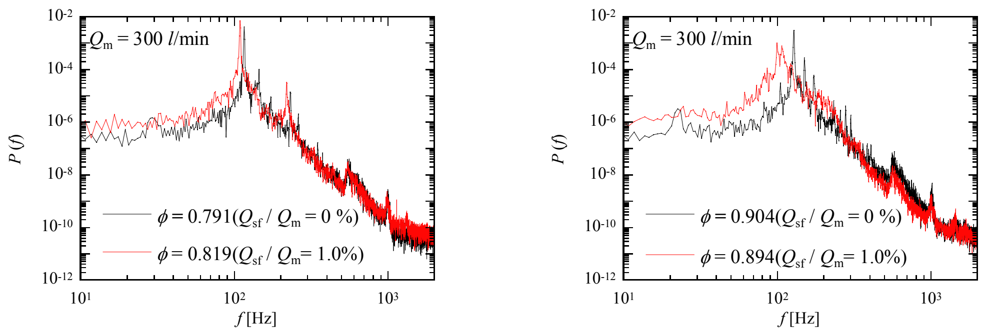

Fig. 4 Power spectrum of pressure fluctuations with and without secondary fuel injection

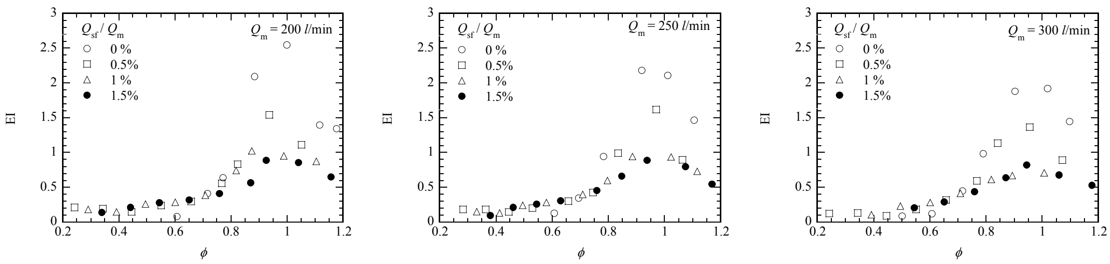

Fig. 5 Emission index with secondary fuel injection

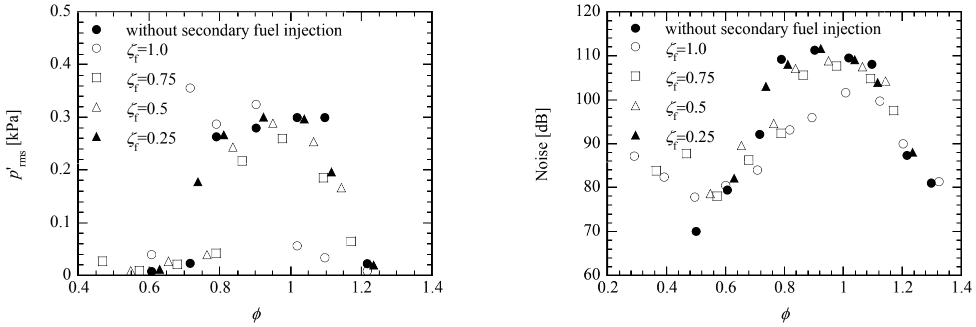

Fig. 6 Effect of secondary premixed mixture injection on pressure fluctuations and noise

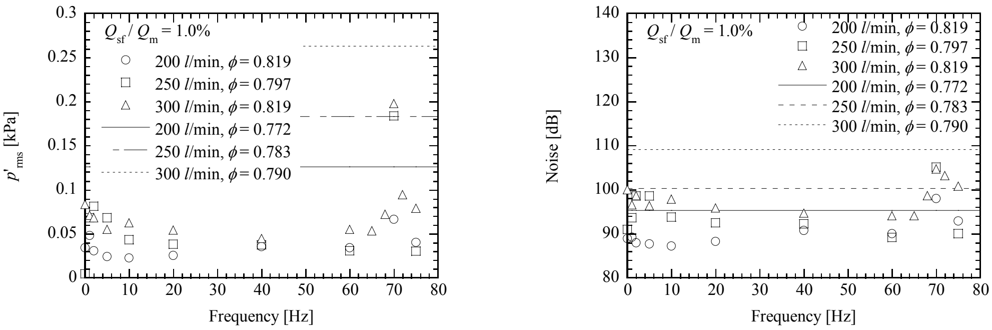

Fig. 7 Effect of injection frequency of secondary fuel on pressure fluctuations and noise

Figure 7 shows the effect of injection frequency of secondary fuel on pressure fluctuations and noise. To compare with conditions without secondary fuel injection, results without secondary fuel injection are also plotted. Regardless of mixture flow rates, r. m. s. of pressure fluctuations show similar tendency and it has minimum value at about 40Hz. Considering that the most of the pressure fluctuations energy is in the region of 117-130Hz, this 40Hz corresponds to one-fourth frequency of the most energetic pressure fluctuations. From the results of the injection frequency effect, it can be seen that the injection frequency of secondary fuel can affect the r. m. s. of pressure fluctuations and noise level in this swirl-stabilized premixed combustor.

3. Measurement of local flame structure in turbulent premixed flames

3.1 Simultaneous measurement of CH/OH PLIF and stereoscopic PIV

The schematic diagram of the experimental setup for simultaneous CH and OH PLIF and stereoscopic PIV measurement is shown in Fig. 8. For CH-PLIF measurement, the $Q_1(7,5)$ transition of the $B^2\Sigma^-$ - $X^2\Pi(0,0)$ band at 390.30nm was excited and fluorescence from the A-X(1,1), (0,0) and B-X(0,1) bands between 420 and 440nm was detected (Garland *et al*. 1985, Carter *et al*. 1998). The fluorescence from the A-X(1,0) and (0,0) bands (306 - 320nm) was collected for OH-PLIF measurement. Details of laser and optical systems were explained in previous study (Tanahashi, et al. 2003b). For PLIF, the laser beam is shaped into 200μm vertical sheet with 30mm height. The CH-OH PLIF system affords a view of 31mm × 31mm. Spatial resolution of PLIF is 31μm × 31μm × 200μm for CH and 61μm × 61μm × 200μm for OH. To optimize signal-to-noise ratio, all measurements were conducted with an image intensifier gate time of 30ns; this value was determined by preliminary experiments with different gate times.

A schematic of stereoscopic PIV is also shown in Fig. 8. This system consists of a double pulsed Nd:YAG laser (New Wave Research, 532nm, 100mJ/6ns), an optical system and two high speed CMOS camera (Vision Research, Phantom V5.0) with 105mm/f2.8 lens. CMOS cameras are located at the both sides of the intensified CCD camera for OH PLIF with ±18 degree to capture stereoscopic particle images. The double-pulsed beams are expanded by the laser sheet optics. The double-pulsed laser sheets illuminate the measuring region and scattered light by tracer particles is recorded by the high-speed CMOS camera of which resolution is 1024 × 1024 pixels at 1000 frames/s and 512 × 512 pixels at 3700 frames/s. For the stereoscopic PIV, the measuring region and the interrogation region are set to 16.2mm × 16.2mm and 24 × 24 pixels, respectively. Since the thickness of the laser sheet is about 1.0mm, spatial resolution of the PIV becomes 759μm × 759μm × 1000μm. As for the tracer particles, 5μm SiO_2, 0.4μm TiO_2 and 0.18μm Al_2O_3 were tested because scattering of CH PLIF excitation laser by the particles contaminates the CH fluorescence image. As the intensity of the scattered light near CH fluorescence seems to depend on

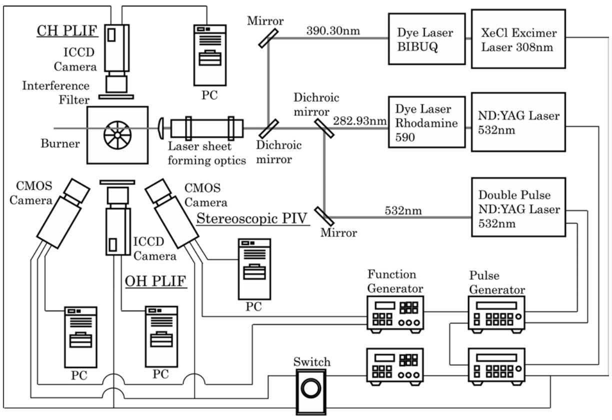

Fig. 8 Schematic of the simultaneous CH-OH PLIF and stereoscopic PIV measurement.

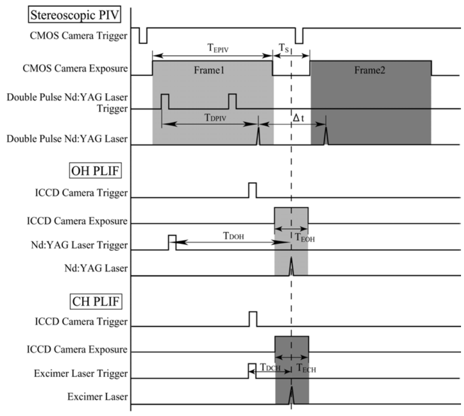

Fig. 9 Timing diagram

the diameter of the particle, Al_2O_3 are used for tracer particles in this study. In this study, a high spatial resolution PIV algorithm developed by our previous study is used to obtain two-dimensional velocity field from successive particle images by each CMOS camera (Tanahashi, *et al*. 2002c) . To ensure the accuracy of the PIV measurement, the elimination scheme of the spurious vectors and noises is established by a PIV simulation based on DNS of particle-laden homogeneous isotropic turbulence. Note that number of the spurious vectors included in the raw data is very few (less than 0.5%) in the present measurements and the elimination scheme is mainly used for cutoff of the high wave number noises which exceed the spatial resolution of PIV. The high wave number noises are introduced by the overlap of the interrogation regions. From two-dimensional velocity fields obtained by each CMOS camera, three component velocity vectors on a two-dimensional plane are calculated by using a geometrical relation (Arroyo, *et al*. 1991, Willert, *et al*. 1997, Prasad, 2000). If high power and high-repetition-rate pulse lasers for industrial processing are adopted as a light source instead of the double pulsed Nd:YAG laser, temporal resolution of this stereoscopic PIV can be several tens of kHz as reported by Tanahashi, et al. (2003a). However, we focus on the simultaneous CH-OH PLIF and stereoscopic PIV measurement because temporal resolutions of PLIF are of the order of several Hz. In Fig. 9, the timing diagram of the simultaneous CH-OH PLIF and stereoscopic PIV measurement is shown. As for the stereoscopic PIV, CMOS cameras are operated with 3.2kHz using 512 × 512 pixels, which results in 302μs exposure time. This high-speed operation was conducted to reject flame radiation and ensure the quality of particle images. The CMOS camera starts to expose 3μs after the negative edge of the trigger. Each laser beam is synchronized to each frame interval. Generally, cameras need the dead time (T_S) to store data between camera frames and the time interval of successive images (Δt) is limited by this dead time. The theoretical minimum T_S of the CMOS camera used in this study is about 5μs. CH and OH PLIF measurements are synchronized to $\Delta t/2$ after the first laser pulse for PIV. Timing controls of this system are conducted by two delay generators (SRS, DG535) and two function generators (SONY Tektronix, AFG320). Time difference error between PLIF and PIV is limited to be less than 100ns, and that between CH PLIF and OH PLIF is controlled to be of the order of 1ns. Based on the characteristics of the turbulent flow field, Δt is set to 15μs.

In this study, the simultaneous CH-OH PLIF and stereoscopic PIV measurements are conducted for three different flow rate: Q_m = 200, 250 and 300 *l*/min for equivalence ratio ϕ = 1.0. To investigate the turbulent characteristics of the unburned mixture, a hot-wire measurements are conducted in inert flows. The simultaneous CH-OH PLIF and stereoscopic PIV measurements were conducted in a cross-section with the maximum u'_{rms}, where u'_{rms} indicates r. m. s. velocity fluctuation. Figure 10 shows overview of swirl-stabilized premixed flame combustor with cameras for simultaneous CH-OH PLIF and stereoscopic PIV measurement and direct photographs of flame. White box in the direct photograph denotes the measurement region of CH and OH PLIF, and box with broken lines represent the measurement region of PIV. Energy spectra of the streamwise velocity at the maximum u'_{rms} point shows -5/3 power law in the inertial subrange and turbulence is fully developed. The turbulence characteristics obtained by the hot-wire measurement were explained in our previous study (Tanahashi, et al. 2003b). With the increase of the flow rate, Re_λ changes from 63.1 to 115.0. All conditions are classified into the corrugated flamelets regime proposed by Peters(1999).

3.2 Fine scale structure of swirl-stabilized premixed flame

Figure 11 shows CH and OH PLIF images obtained in two different realizations for Re_λ =115.0(Q_m=300 *l*/min). In this figure, red color denotes high concentration and white line represent integral length scale of turbulence. CH and OH radicals show very complicated distributions. The edge of OH radical concentration coincides with CH layer very well.

Flame fronts show large scale wrinkling of the order of the integral length scale and small scale wrinkling less than Taylor micro scale. From comparisons of CH and OH radical distribution, isolated burned gas in the unburned mixture(see circle A) and isolated unburned mixture in the burned side(see circle B) can be observed even in the corrugated flamelet regime. Appearrance of the isolated unburned mixture has been shown by Chen, *et al.* (1999), Tanahashi, *et al.*(2001) and Saito, *et al.*(2002) from two-dimensional DNS.

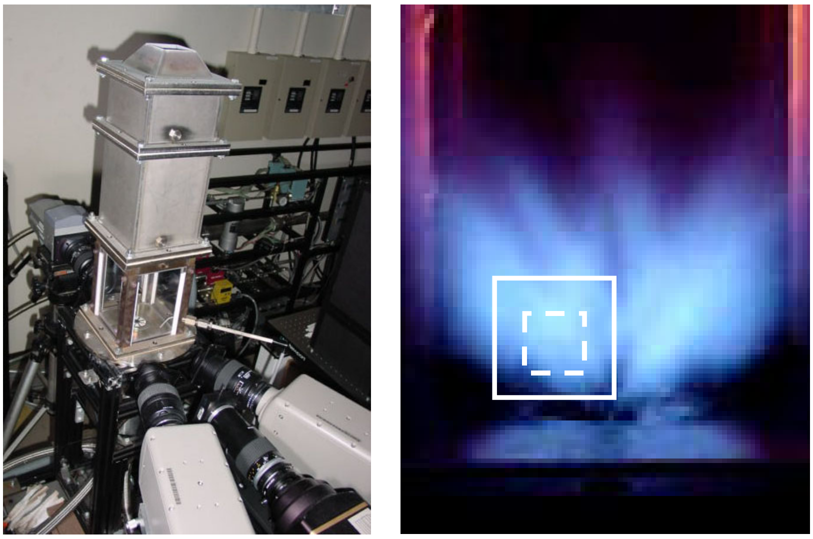

(a) Overview of combustor (b) Measuring region

Fig. 10 Overview of swirl-stabilized combustor and measuring region in the flame

Three-dimensional DNS by Nada et al(2003) showed that the isolated unburned mixture reflects one feature of three-dimensional flame structure, which is called as the handgrip structure. The isolated burned gas in the unburned side is also predicted by DNS of hydrogen-air and methane-air turbulent premixed flame(Tanahashi, *et al.* 2001, Saito, *et al.* 2002). These results suggest that the simultaneous CH and OH PLIF is important in high Renolds number turbulence because these flame structures can not be recognized by single radical PLIF.

In Fig. 12, CH and OH PLIF images are presented with a velocity field for Re_λ =95(Q_m=250 l/min). The velocity vectors in the measurement plane are overlaid on CH and OH PLIF images. Velocity across the measurement plane is shown by white and grey with velocity vector in the measurement plane, and its unit is m/s. Comparisons of CH-OH PLIF and three-dimensional velocity field imply that the burned gases not always shows high speed in relatively high Reynolds number turbulent premixed flame, which may caused by multiply folded flame structure and the large scale recirculation region behind the swirler. Since negative velocity across the measurement plane is scarcely observed in the inert flow with the same flow rate, the velocity field is significantly affected by the presence of the flames. Figure 13 shows CH and OH PLIF images and three component velocities for different Reynolds number. White boxes in CH PLIF images represent the stereoscopic PIV measurement region displayed in the right hand side.

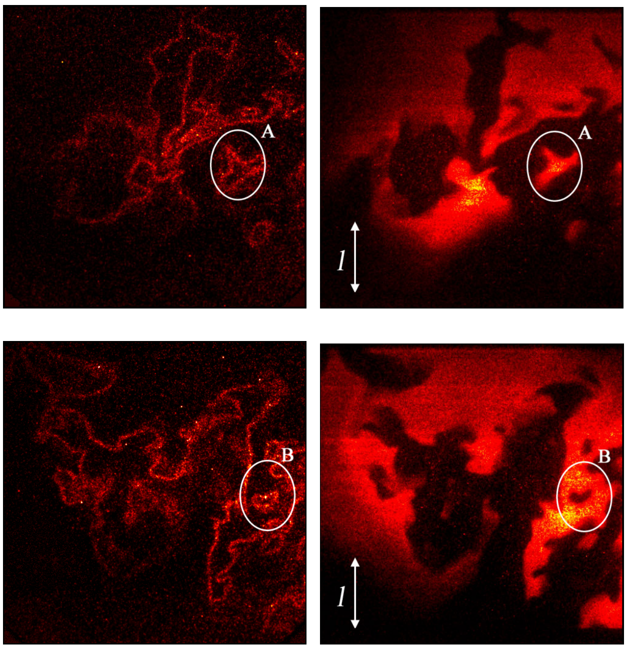

Fig. 11 Simultaneous fluorescence images of CH radicals (right) and OH radicals (left) for Re_λ = 115.0 (Q_m = 300 l/min). Top and bottom images represents different realization.

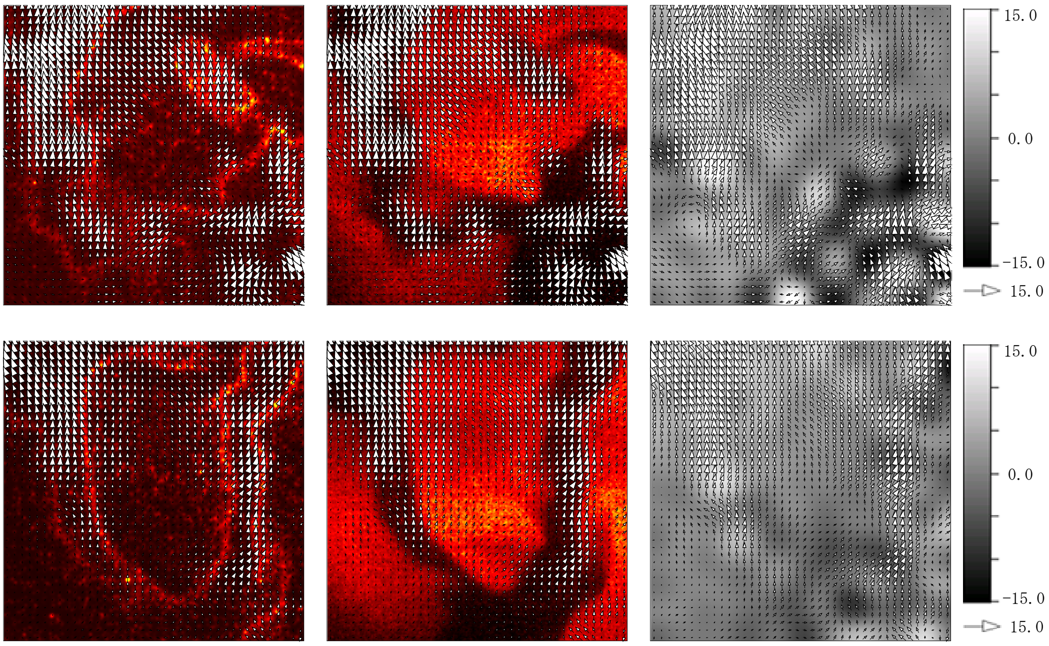

Fig. 12 Velocity vectors in the measurement plane with CH PLIF image (left), OH PLIF image (center) and velocity distribution across the plane (right) for $Re_\lambda = 95.0$. Top and bottom images represents different realization.

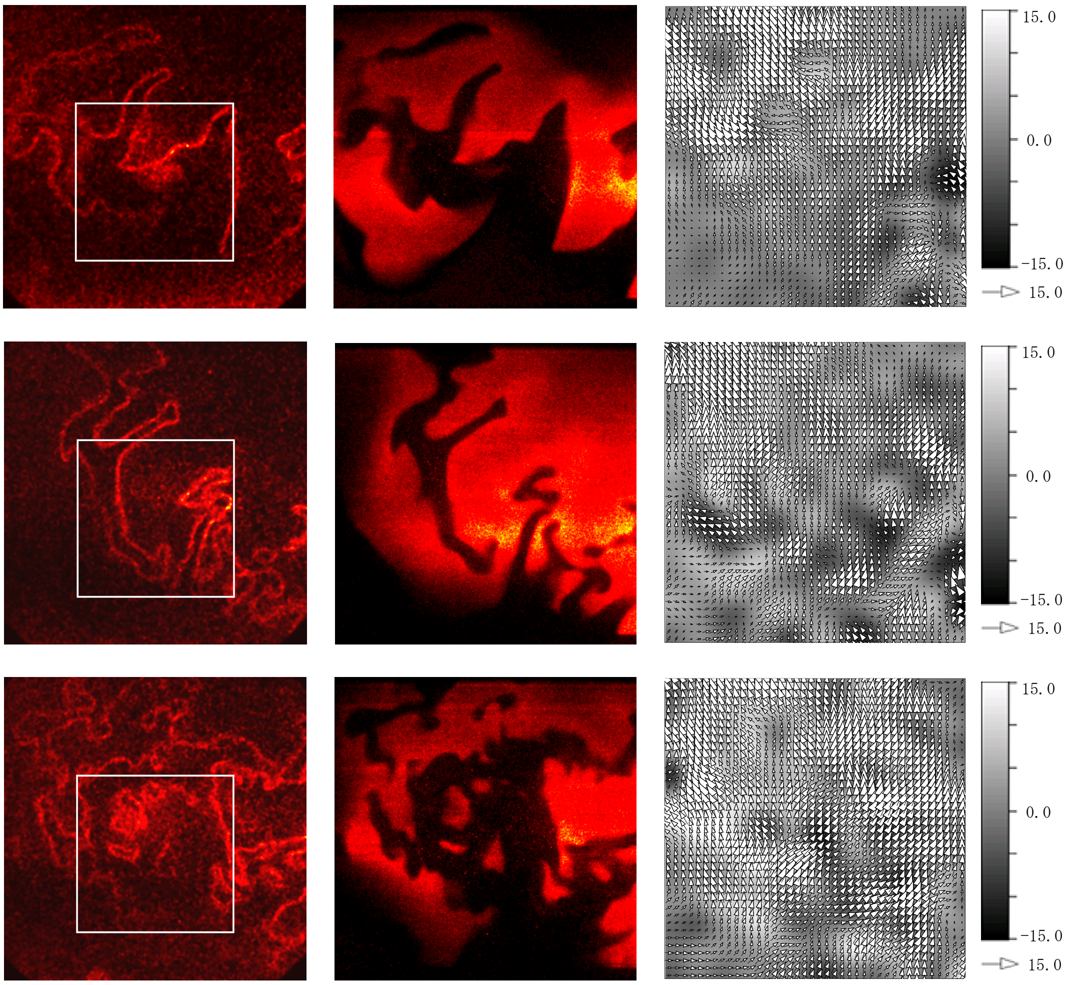

Fig. 13 Reynolds number dependence of CH PLIF image (left), OH PLIF image (center) and velocity distribution (right). $Re_\lambda = 63.5$ (Top), $Re_\lambda = 95.0$ (Middle) and $Re_\lambda = 115.0$ (Bottom)

With the increase of Reynolds number, number of wrinkles of flame front increases significantly and flame front show very complicated geometry. Three-dimensional DNS(Tanahashi, *et al*. 2000, 2002b, Nada, *et al*. 2003) and fractal analysis of OH PLIF results conducted in high pressure turbulent premixed flames (Kobayashi, *et al*. 2002) showed that the smallest curvature radius of the flame front is of the order of Kolmogorov micro scale of the unburned mixture. As the Kolmogorov micro scale in the present study does not change so much (Tanahashi, *et al*. 2003b), the observation in Fig. 13 shows that the flame surface density increases wuth the increase of Reynolds number.

4. Summary

In this study, control of oscillating combustion with secondary fuel injection has been studied to reduce the pressure fluctuations, combustion noise and emission index and prevent lean blow out. In addition, simultaneous CH-OH PLIF and stereoscopic PIV measurement method has been established to measure local flame structure of relatively high Reynolds number turbulence flames. From the combustion control of oscillating flames with secondary fuel injection, pressure fluctuations can be controlled by secondary fuel injection, and this control is effective in suppression of combustion oscillation, prevention of lean blowout and reduction of emission index in the present swirl premixed combustor. Secondary premixed mixture injection is not effective for control of combustion oscillations and lean blowout prevention. The minimum value of r. m. s. of pressure fluctuations and noise has been observed when the secondary fuel was injected at 40Hz, which corresponds to one-fourth frequency of the most energetic pressure fluctuations.

In the development of simultaneous CH-OH PLIF and stereoscopic measurement method, high-speed CMOS cameras were adopted to capture the clear stereoscopic particle images without contamination by the flame radiation. The developed simultaneous two radical concentrations and three component velocity measurement on a two-dimensional plane was applied for relatively high Reynolds number turbulent premixed flames in a swirl-stabilized combustor. All measurements were conducted for methane-air premixed flames in the corrugated flamelets regime. Simultaneous CH and OH images suggest that the presence of the isolated burned gas in the unburned mixture and the isolated unburned mixture in the burned side which have been predicted by DNS. Comparisons of CH-OH PLIF and three-dimensional velocity field show that the burned gases not always have high-speed velocity in relatively high Reynolds number turbulent premixed flame. The Reynolds number dependence of frame front geometry was clearly captured by the simultaneous CH-OH PLIF and stereoscopic PIV measurement.

References

Allen, M., Howe, R. D. and Hanson, R. K., (1986), *Opt. Lett*., 11: 126-128.

Arroyo, M. P. and Greated, C. A., (1991), *Meas. Sci. Technol*., 2: 1181-1186.

Bell, J. B., Day, M. S. and Grcar, J. F., (2002), *Proc. Combust. Inst.*, 29: 1987-1993.

Blonbou, R., Laverdant, A., Zaleski, S., and Kuentzmann, P., (2000), *Proc. Combust. Inst*., 28:747-755.

Bockle, S., Kazenwadel, J., Kunzelmann, T., Shin D.-I., Schulz, C. and Wolfrum, J., (2000), *Proc. Combust. Inst.*, 28: 279-286.

Broda, J. C, Seo, S., Santoro, R. J., Shirhattikar, G., and Yang, V., (1998), *Proc. Combust. Inst*., 27:1849-1856.

Carter, C. D., Donbar, J. M. and Driscoll, J. F., (1998), *Appl. Phys.*, B, 66: 129-132.

Chen, J., Echekki, T. and Kollomann, W., (1999), *Combust. Flame*, 116: 15-48.

Delabroy, O., Haile, E., Lacas, F., Candel, S., Pollard, A., Sobiesiak, A., Becker, H. A., (1998), *Exp. Thermal Fluid Sci.*, 16:64-75.

Di Benedetto, A., Marra, F. S., and Russo, G., (2002), *Sci. and Tech*., 174(10):1-18.

Donbar, J. M., Driscoll, J. F. and Carter, C. D., (2000), *Combust. Flame*, 122: 1-19.

Dyer, M. J. and Crosley, D. R., (1985), *Proc. Int. Conf. on Laser '84*, pp. 211-218.

Garland, N. L., and Crosley, D. R., (1985), *Appl. Optics*, 24: 4229-4237.

Gulati, A., and Mani, R., (1992), *J. Prop. Power* 8(5):1109-1115.

Han, D., and Mungal, M. G., (2000), *Proc. Combust. Inst*., 28: 261-267.

Hanson, R. K., (1986), *Proc. Combust. Inst.*, 21: 1677-169.

Harper, J., Johnson, C. J., Neumeier, Y., Lieuwen, T., and Zinn, B. T., *AIAA Paper* #2001-0486.

Hong, B-S., Ray, A., and Yang, V., (2002), *Combust. Flame*, 128:242-258.

Jenkins, K. W. and Cant, R. S., (2002), *Proc. Combust. Inst*., 29: 2023-2029.

Kalt, P. A. M., Frack, J. H. and Bilger, R. W., (1998), *Proc. Combust. Inst*., 27: 751-758.

Kobayashi, H., Kawabata, T., Seyama, K., Fujimari, T. and Kim, J. S., (2002), *Proc. Combust. Inst*., 29: 1793-1799.

Kothnur, P. S., Tsurikov, M. S., Clemens, N. T., Donbar, J. M. and Carter, C. D., (2002), *Proc. Combust. Inst*., 29: 1921-1927.

Lee, J. G., Kim, K., and Santavicca, D., (2000), *Proc. Combust. Inst.*, 28:739-746.
Lieuwen, T., and Zinn, B. T., (2000), *AIAA paper*, #2000-0707.
Mansour, M. S., Peters, N. and Chen, Y. C., (1998), *Proc. Combust. Inst.*, 27: 767-773.
Murugappan, S., Gutmark, E. J., Acharya, S., and Kristic, M., (2000), *Proc. Combust. Inst.*, 28:731-737.
Nada, Y., Tanahashi, M. and Miyauchi, T., (2003), *Proc. 3th Int. Conf. Turbulence and Shear Flow Phenomena*, 2: 579-584 (submitted to J. Turbulence).
Paschereit, C. O., Gutmark, E., and Weisenstain, W., (1999), *Physics of Fluids*, 11(9):2667-2678.
Paul, P. H. and Najm, H. N., (1998), *Proc. Combust. Inst.*, 27: 43-50.
Peters, N., (1999), *J. Fluid Mech.*, 384: 107-132.
Poinsot, T., Le Chatelier, C., Candel, S. M., and Esposito, E., (1986), *J. Sound Vibr.*, 107(2):265-278.
Poppe, C., Sivaegaram, S., and Whitelaw, J. H., (1998), *Combust. Flame*, 113:13-26.
Prasad, A. K., (2000), *Exp. Fluids*. 29: 103-116.
Rayleigh, L. *Theory of Sound*, Dover, New York, 1945.
Rehm, J. E., Clemens, N. T., (1998), *Proc. Combust. Inst.*, 27: 1113-1120.
Saito, T., Tanahashi, M. and Miyauchi, T., (2002), *J. Combust. Society of Japan*, 44: 243-252.
Samaniego, J. M., Yip, B., Poinsot, T., and Candel, S., (1993), *Combust. Flame*, 94:363-380.
Sinibaldi, J. O., Driscoll, J. F., Mueller, C. J., Donbar, J. M. and Carter, C. D., (2002), *Combust. Flame*, 133: 323-334.
Sivasegaram, S., Tsai, R. F., and Whitelaw, J. H., (1995), *Combust. Sci. Technol*. 10(5):67-83.
Sreedhara, S. and Lakshmisha, K. N., (2002), *Proc. Combust. Inst*.. 29: 2051-2059.
Tanahashi, M., Fujimura, M. and Miyauchi, T., (2000), *Proc. Combust. Inst*., 28: 529-535.
Tanahashi, M., Fukuchi, Y., Choi, G.-M., Fukuzato, K. and T. Miyauchi, (2003a), *in Proc. Turbulence, Heat and Mass Transfer* 4, 245-252.
Tanahashi, M., Li, Y., Choi, G-M., and Miyauchi, T., (2002a), *9th Int. Conf. Numerical Combustion*, pp. 201-202.
Tanahashi, M., Nada, Y., Ito, Y. and Miyauchi, T., (2002b), *Proc. Combust. Inst*., 29: 2041-2049.
Tanahashi, M., Nada, Y., Tsukinari, S. Saitoh, T. Miyauchi, T. and Choi, G.-M., (2003b), *Proc. the 4th Sym. Smart Control of Turbulence*, pp. 81-91.
Tanahashi, M., Ootsu, M., Fukushima, M. and Miyauchi, T., (2002c), *Engineering Turbulence Modeling and Measurements 5*, Elsevier, pp. 525-534.
Tanahashi, M., Yu, Y. and Miyauchi, T., (2001), *Trans. JSME*, 67:563-543.
Watson, K. A., Lyons, K. M., Carter, C. D. and Donbar, J. M., (2002), *Proc. Combust. Inst*., 29: 1905-1912.
Watson, K. A., Lyons, K. M., Donbar, J. M., and Carter, C. D., *Combust. Flame*, (2000), 123: 252-265.
Willert, C., (1997), *Meas. Sci. Technol*., 8: 1465-1479.